Magnetic structures of cubic FeGe studied by small-angle neutron scattering

1989 J. Phys.: Condens. Matter 1 6105

(http://iopscience.iop.org/0953-8984/1/35/010)

J. Phys.: Condens. Matter 1 (1989) 6105–6122. Printed in the UK

Magnetic structures of cubic FeGe studied by small-angle neutron scattering

B Lebech†, J Bernhard‡ and T Freltoft†§

† Physics Department, Risø National Laboratory, DK-4000 Roskilde, Denmark

‡ Department of Solid State Physics, Institute of Technology, Uppsala University, S-75121 Uppsala, Sweden

Received 23 January 1989

Abstract. The magnetic ordering of a single crystal of the cubic polymorph of FeGe has been studied by small-angle neutron scattering. The compound orders magnetically at T_N = 278.7 K into a long-range spiral (period ~ 683–700 Å) propagating along equivalent ⟨100⟩ directions at high temperatures and along equivalent ⟨111⟩ directions at low temperatures. The length of the spiral wavevector is nearly independent of temperature. The transition at T_N is first order with very little hysteresis. The transition at which the direction of the spiral turns is rather sluggish. It takes place in a temperature interval of ~40 K and shows pronounced temperature hysteresis ($T_{2\downarrow}$ = 211 K, $T_{2\uparrow}$ = 245 K). Applied magnetic fields of 20–40 mT, depending on the temperature and the field direction, cause the spiral axis to turn into the direction of the applied field. As the field is further increased, the amplitude of the antiferromagnetic spiral decreases and the ferromagnetic component increases until at fields above ~200–300 mT cubic FeGe becomes magnetically saturated. The magnetic ordering in cubic FeGe is a Dzyaloshinskii spiral similar to the structure observed in the isostructural compound MnSi. However, in MnSi the spiral propagates along equivalent ⟨111⟩ directions at all temperatures below T_N = 29.5 K.

1. Introduction

For a number of years it has been known that the magnetic structures in certain crystals lacking inversion symmetry may be very-long-range periodic structures, the so-called Dzyaloshinskii spirals (Dzyaloshinskii 1964). The mechanism causing this long-range magnetic superstructure is the instability of a ferromagnetic structure with respect to small 'relativistic' spin–lattice or spin–spin interactions. Nakanishi *et al* (1980) and Bak and Jensen (1980) made a symmetry analysis of the $P2_13$ structure and showed that a helical magnetic structure may indeed occur in $P2_13$ as a consequence of the Dzyaloshinskii instability. In these analyses, the free energy was expanded in terms of a slowly varying spin density ($\boldsymbol{S}(\boldsymbol{r})$), and Bak and Jensen (1980) found that the magnetic structure is a right-handed or left-handed spiral propagating along $q \parallel \langle 111 \rangle$† for $B_2 < 0$ and along

§ Present address: NKT A/S, Department of Corporate Research and Development, DK-2605 Brøndby, Denmark.

† Throughout the paper, we use the notation ⟨*hkl*⟩ for all equivalent symmetry directions, [*hkl*] for a particular direction in reciprocal space and (*hkl*) for a Bragg point or a reciprocal lattice vector. For the spiral wavevector we use q (or $\boldsymbol{q}$) when the length is quoted in relative (100) reciprocal lattice units (RLU) and Q (or $\boldsymbol{Q}$) for the spiral wavevector in Å^{-1}.

0953-8984/89/356105 + 18 $02.50

$q \parallel \langle 100 \rangle$ for $B_2 > 0$, where B_2 is the second-order gradient term in the free energy expansion. Bak and Jensen (1980) also studied the nature of the phase transition by means of renormalisation group theory. They found that for a Dzyaloshinskii spiral structure in a $P2_13$ structure the transition to the magnetically ordered state should be of first order.

The intermetallic compound iron monogermanide (FeGe) crystallises in three polymorphs with monoclinic ($a = 11.838$ Å, $b = 3.936$ Å, $c = 4.934$ Å), hexagonal ($a = 5.003$ Å, $c = 4.055$ Å) and cubic ($a = 4.700$ Å) crystal structures (Richardson 1967) which order antiferromagnetically below 342, 410 and 278 K, respectively (Felcher *et al* 1983, Fruchart *et al* 1983, Bernhard *et al* 1984, 1988, Wilkinson *et al* 1976). The cubic polymorph is isostructural with cubic MnSi. Both compounds crystallise in the tetrahedrally coordinated T_4 ($P2_13$) structure of FeSi, with atoms in the (4*a*) positions, (x, x, x); $(\frac{1}{2}+x, \frac{1}{2}-x, x)$; $(x, \frac{1}{2}+x, \frac{1}{2}-x)$; $(\frac{1}{2}-x, x, \frac{1}{2}+x)$, where $x_{Fe} = 0.137$ and $x_{Si} = 0.842$ (Pauling and Soldate 1948). As mentioned above, the $P2_13$ structure lacks inversion symmetry, and both cubic FeGe and MnSi are possible candidates as compounds exhibiting magnetic structures of the Dzyaloshinskii type. Prior to this work, the magnetic properties of both cubic FeGe and MnSi have been studied by classical techniques. In addition the magnetism has been studied by neutron diffraction on single crystals of MnSi and on a powder of cubic FeGe. The reason for this difference is that it is relatively easy to grow large single crystals of MnSi, but difficult to grow single crystals of cubic FeGe.

The present work describes the first neutron diffraction study of the magnetic ordering of a single crystal of cubic FeGe, revealing the details of the Dzyaloshinskii spiral at various temperatures between $T_N = 278.7$ and 25 K with and without applied magnetic fields. Because of the very-long-range magnetic spiral structures found in cubic FeGe, the study was made by means of small-angle neutron scattering which is a novel, although somewhat limited, technique for studying magnetic structures. Below we describe the experimental details (§ 2) and the experimental results in zero field (§ 3) and in applied fields (§ 4). In § 5 we give a summary and discuss the magnetic ordering in cubic FeGe and related compounds.

Before describing the present work we review briefly the earlier results of studies of the magnetic properties of cubic FeGe and, for completeness, for the isostructural related compound MnSi. For historical reasons, we start by reviewing the results for MnSi.

1.1 Review of magnetic studies of MnSi

The magnetic phase diagram of MnSi was studied by various experimental methods such as magnetisation (Levinson *et al* 1978, Bloch *et al* 1975, Hansen 1977), ultrasonic attenuation (Kusaka *et al* 1976), neutron diffraction (Ishikwa *et al* 1976, 1977, Hansen 1977, Ishikawa and Arai 1984), ESR measurements (Date *et al* 1977) and other techniques (Sakakibara 1982). In zero field, cubic MnSi orders magnetically through a first-order transition (Hansen 1977) at $T_N = (29.5 \pm 0.05)$ K into a helical spin structure with wavevectors $Q = 0.036$ Å^{-1} along equivalent $\langle 111 \rangle$ directions (Ishikawa *et al* 1976, Lebech and Hansen 1977). Except for a slight increase near T_N (Hansen 1977, Ishikawa *et al* 1984), the wavevector is nearly independent of temperature. Both the first-order transition at T_N and the long-range Dzyaloshinskii-type spiral magnetic structure found in MnSi (periodicity ~ 175 Å or ~39 unit cells) are consistent with the predictions of theory (Nakanishi *et al* 1980, Bak and Jensen 1980). In an applied magnetic field the

propagation vector of the spiral rotates into the field direction without changing its length (Ishikawa *et al* 1976, Plumer and Walker 1981). The amplitude of the spiral structure decreases with increasing field, and MnSi becomes magnetically saturated at 600 mT (Levinson *et al* 1978, Bloch *et al* 1975).

1.2. Review of previous magnetic studies of cubic FeGe

Mössbauer (Wäppling and Häggström 1968, Ericsson *et al* 1981) and magnetisation data (Lundgren *et al* 1968, 1970) showed that cubic FeGe orders magnetically at ~280 K, and the similarity between the magnetisation data of MnSi and cubic FeGe as well as the crystal structure predict that cubic FeGe orders in a spiral structure like that observed in MnSi. The existence of a Dzyaloshinskii-type magnetic structure in cubic FeGe was confirmed by the small-angle neutron scattering measurements of Wilkinson *et al* (1976) on a powdered sample of cubic FeGe. At 120 K they observed a ring of scattering at a distance of 0.0092 $Å^{-1}$ from the origo. This corresponds to a spiral with a repeat distance of 700 Å (~149 unit cells). However, because Wilkinson *et al* (1976) studied a powder, they could not determine the direction in which the spiral propagates. Application of a magnetic field of 330 mT caused the ring-formed scattering to elongate and collapse into sharp diffraction spots. This was interpreted as evidence of a turn of the spiral propagation vector into the field direction. The ESR measurements by Haraldson *et al* (1978) on a single crystal of cubic FeGe showed three resonance lines having temperature and field dependencies similar to those observed in MnSi by Date *et al* (1977). Haraldson *et al* (1978) interpreted their data in terms of a spiral magnetic structure which is equally hard in any direction, because only a small field (10–20 mT) is needed to turn the spiral axis into the field direction, whereas a comparatively large (field (~200 mT) is needed to cause magnetic saturation.

2. Experimental details

The measurements were carried out at the small-angle neutron scattering facility (SANS) situated at a cold source neutron beam outside the reactor confinement of the DR3 steady-state reactor at Risø. The instrument (Kjems *et al* 1985a, b) uses neutron wavelengths in the range 4 to 24 Å with momentum transfers in the range 0.2 to 0.003 $Å^{-1}$. The monochromatisation is provided by a mechanical velocity selector with variable tilt to control resolution. In the present experiment, we used $\Delta\lambda/\lambda \simeq 0.18$ full width at half maximum. The main part of the data were collected using incident neutrons of wavelength 15.8 Å, which means that all scattering within a square reciprocal lattice area of 0.04×0.04 $Å^{-2}$ around the origo is recorded by the 40×40 cm^2 area-sensitive neutron detector (Kjems *et al* 1985a). Two collimating diaphragms (16 and 5 mm in diameter) define the incoming beam. A beam monitor is placed just after the diaphragms. The main function of the monitor is to compensate for variations in reactor flux and to allow a meaningful comparison between successive experiments. A moveable beam stop (40 mm diameter) is placed in the direct beam just in front of the area-sensitive detector.

The single crystal of cubic FeGe was grown by Richardson using a method (Richardson 1967) based on a halogen chemical transport reaction. The crystal is of a somewhat irregular shape which can be approximated to a flattened sphere of diameter 1 mm.

Before mounting the FeGe crystal in the SANS instrument, it was oriented and characterised at the Risø four-circle neutron diffractometer using incident neutrons of

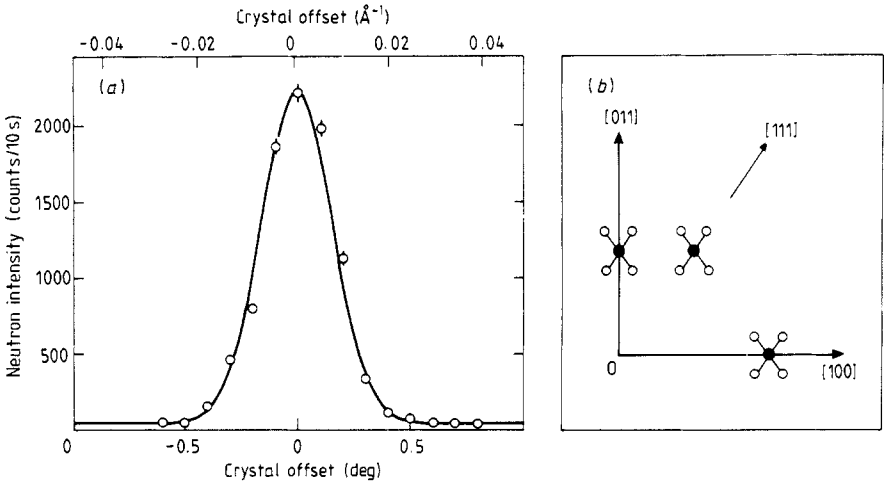

Figure 1. (*a*) Crystal rocking curve for the (2, 0, 0) Bragg peak of cubic FeGe, measured with a conventional neutron spectrometer using incident neutrons of wavelength 2.54 Å (FWHM) = 0.38° or 0.018 Å^{-1}). (*b*) Section of reciprocal space showing the (2, 0, 0), (0, 1, 1) and (1, 1, 1) nuclear Bragg reflections and the satellites around them at 10 K. Note that the magnetic satellite wavevector q is not to scale.

wavelength of 1.012 Å. A full-matrix least-squares refinement with isotropic extinction correction resulted in $a = 4.689$ Å, $x_{Fe} = (0.135 \pm 0.001)$ and $x_{Ge} = (0.842 \pm 0.01)$ for FeGe ($R(F) = 8.6\%$, $R(F^2) = 13\%$). Furthermore a search for magnetic satellites at 10 K was made using a high-resolution triple-axis neutron spectrometer with incident neutrons of wavelength 2.54 and 4 Å. Despite numerous attempts with different choices of collimations in the incident and scattered beams, it was not possible to observe and resolve the magnetic reflections around the innermost Bragg reflections ((0, 1, 1), (1, 1, 1), (2, 0, 0) and (2, 1, 0)). Figure 1(*a*) shows a rocking curve for the (2, 0, 0) Bragg reflection obtained using incident neutrons at 2.54 Å. The rocking curve has a full width at half maximum of 0.38° or 0.018 Å^{-1}. It is therefore obvious that magnetic satellites at ± 0.009 Å^{-1} from (2, 0, 0) cannot be observed because they lie on top of the tails of the very intense (2, 0, 0) nuclear Bragg peak (see figure 1(*b*)). Although the (0, 1, 1) reflection is somewhat closer to the origo than (2, 0, 0) with a slight increase of resolution, the (0, 1, 1) is much weaker than the (2, 0, 0) ($\sim 4\%$ $|F(2, 0, 0)|^2$). This means that the (0, 1, 1) satellites (see figure 1(*b*)) are too weak to be observed even if they could be resolved. Similar data from 4 Å incident neutrons led to the same conclusion. Therefore, the SANS technique offers at present the only possible means of studying the magnetic structure of cubic FeGe, despite the obvious drawback that the measured intensities cannot be converted to magnetic moments, because it is not possible to scale the intensities to a suitable nuclear Bragg peak.

As a further check, test experiments with the same spectrometer configurations on the related cubic compound MnSi at 10 K (1 mm diameter spherical single crystal) showed well resolved, relatively intense satellites around the (0, 1, 1) and (1, 2, 0) Bragg reflections, and a (2, 0, 0) rocking curve of similar width as found for the FeGe crystal. A full-matrix refinement with isotropic extinction correction of the four-circle neutron diffraction data for MnSi resulted in $a = 4.558$ Å, $x_{Mn} = (0.138 \pm 0.002)$ and $x_{Si} = (0.845 \pm 0.001)$ ($R(F) = 6.5\%$, $R(F^2) = 14\%$).

For the SANS experiment, the FeGe crystal was mounted with either a [011] or a [100] axis parallel to the incident beam (figure 2) and placed either in the SANS standard sample changer with Peltier cooling/heating or on the cold finger of a He cryostat or a Displex. The cooling device was mounted directly in the high-vacuum system ($\sim 10^{-6}$ mbar) of the SANS instrument through the top of the sample chamber. Using a suitably chosen cooling device, the temperature could be varied continuously and controlled to an accuracy of ± 0.05 K in the temperature range 5 to 300 K. The sample temperature was monitored by a calibrated Ge ($T < 60$ K) or a 100 Ω platinum resistance thermometer. The magnetic fields were produced by a conventional electromagnet which could be placed at the bottom of the SANS sample chamber. For low fields the iron yoke was removed. The field was applied perpendicular to the incident beam, either vertically or horizontally and it was calibrated *in situ* using a Hall probe.

3. Experimental results in zero field

The first measurements in zero magnetic field were carried out with the crystal oriented with the $[0\bar{1}1]$ direction parallel to the incident beam so that the two-dimensional small-angle scattering pattern recorded by the area-sensitive detector displays the scattering in the plane defined by the [100] and [011] reciprocal lattice vectors. The experimental set-up is shown schematically in figure 2, which also illustrates the characteristic diffraction patterns observed below T_N (figure 2(*a*), $T > T_2$; figure 2(*b*), $T < T_2$). The experimentally observed two-dimensional data are shown in figure 3 for various temperatures. The figure shows contours of equal intensity plotted on a logarithmic scale. The contours marked 1 to 3 correspond to intensities equal to 10^5, 10^6 and 10^7, respectively. The counting time for each pattern was 6 min. The intensity data (minus background) have been scaled to the same monitor count and normalised to the incoherent scattering from a water sample in order to correct for detector efficiency. The background (total background ~ 1200 counts min^{-1}, 64×64 channels) was determined as the scattering pattern from the sample at 289 K, i.e. well above the Néel temperature of 278.7 K.

At 278.86 K (see figure 3), just above the Néel temperature, a circular ring of diffuse scattering is observed which increases in intensity as T_N is approached. At 278.63 K, just below T_N, satellites appear at $\boldsymbol{Q}_1 = \pm Q_0(1, 0, 0)$, where $Q_0 = 0.0090$ Å^{-1} (see figure 6). However, a slightly deformed (elliptical) ring of scattering is observed until about 1 K below T_N. At 277.61 K, the satellites at $Q_1 = \pm Q_0(1, 0, 0)$ have grown to nearly full intensity and the scattering pattern appears more or less unchanged with decreasing temperature, down to 232.0 K, where a second magnetic transition starts. The intensity contours broaden in the [011] direction, the distinct satellites disappear and the intensity contours become almost circular (207.60 K, see figure 3), although the scattering is much more intense than the diffuse scattering observed just above T_N. As the temperature is lowered further, the intensity contours become square and eventually at 190.55 K (figure 3), satellites appear at $\boldsymbol{Q}_1 = \pm (Q_0\sqrt{3})\ (1, 1, 1)$ and $\boldsymbol{Q}_2 = \pm (Q_0/\sqrt{3})\ (\bar{1}, 1, 1)$, where $Q_0 = 0.0092$ Å^{-1} at 100 K (see figure 6). The intensity of these satellites increases with decreasing temperature and at the lowest temperatures higher-order satellites develop. A similar temperature dependence is observed with increasing temperature although the transition region is shifted towards higher temperatures.

We interpret the data in terms of a spiral structure propagating along equivalent ⟨100⟩ directions at high temperatures and along equivalent ⟨111⟩ directions at low temperatures. The magnetic moment is perpendicular to the propagation direction of

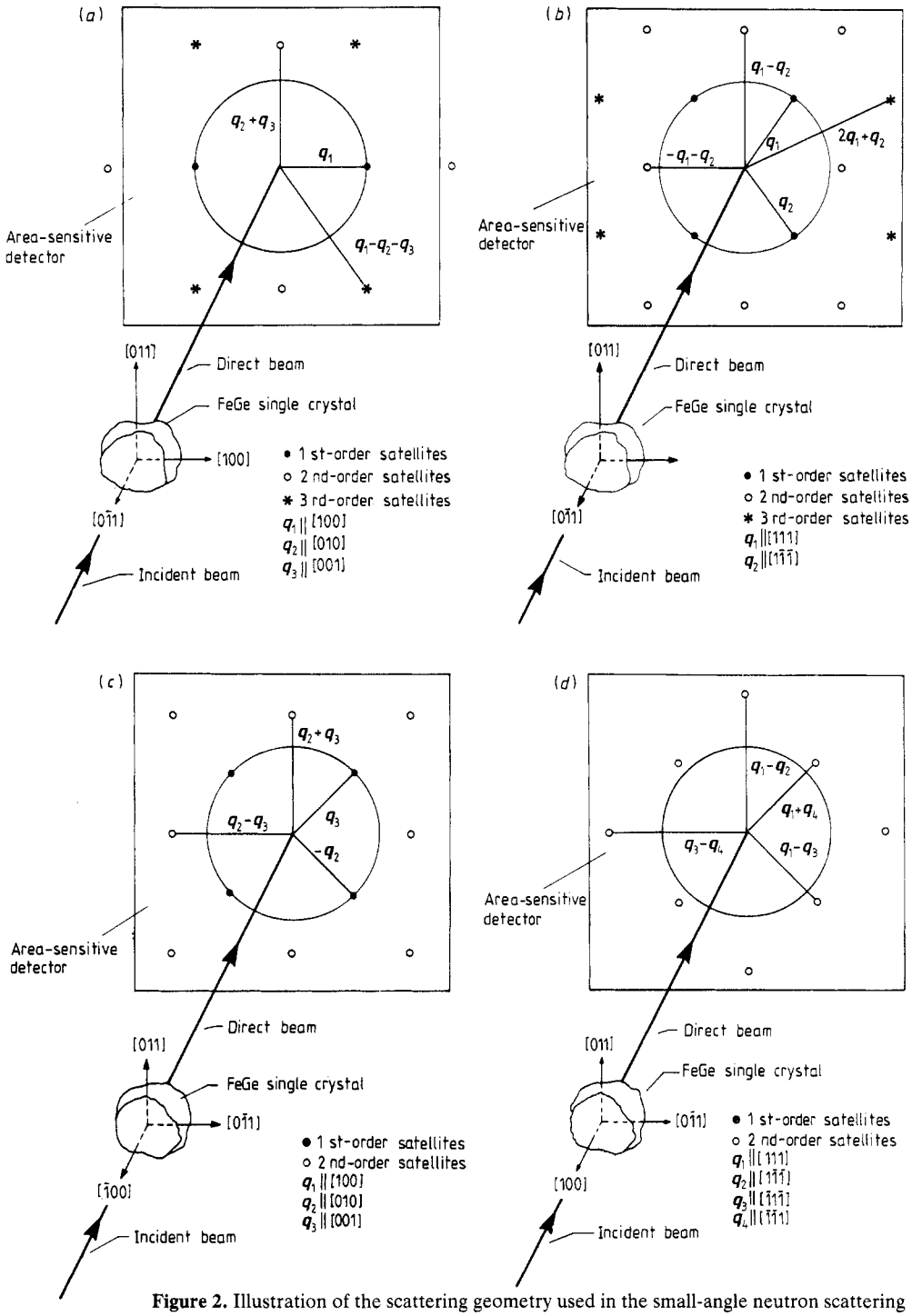

Figure 2. Illustration of the scattering geometry used in the small-angle neutron scattering measurements on cubic FeGe. The positions of the magnetic satellites observed around (0, 0, 0) in the (0$\bar{1}$1) lattice plane ((*a*) and (*b*)) and in the (100) lattice plane ((*c*) and (*d*)) are shown schematically. For $T > T_2$ the wavevectors $\boldsymbol{q}$ of the modulated magnetic structure are parallel to the equivalent ⟨100⟩ direction. For $T < T_2$ the $\boldsymbol{q}$ are parallel to equivalent ⟨111⟩ directions. The circle surrounding the centre of the detector illustrates that the length of $\boldsymbol{q}$ is independent of temperature and the direction of $\boldsymbol{Q}$.

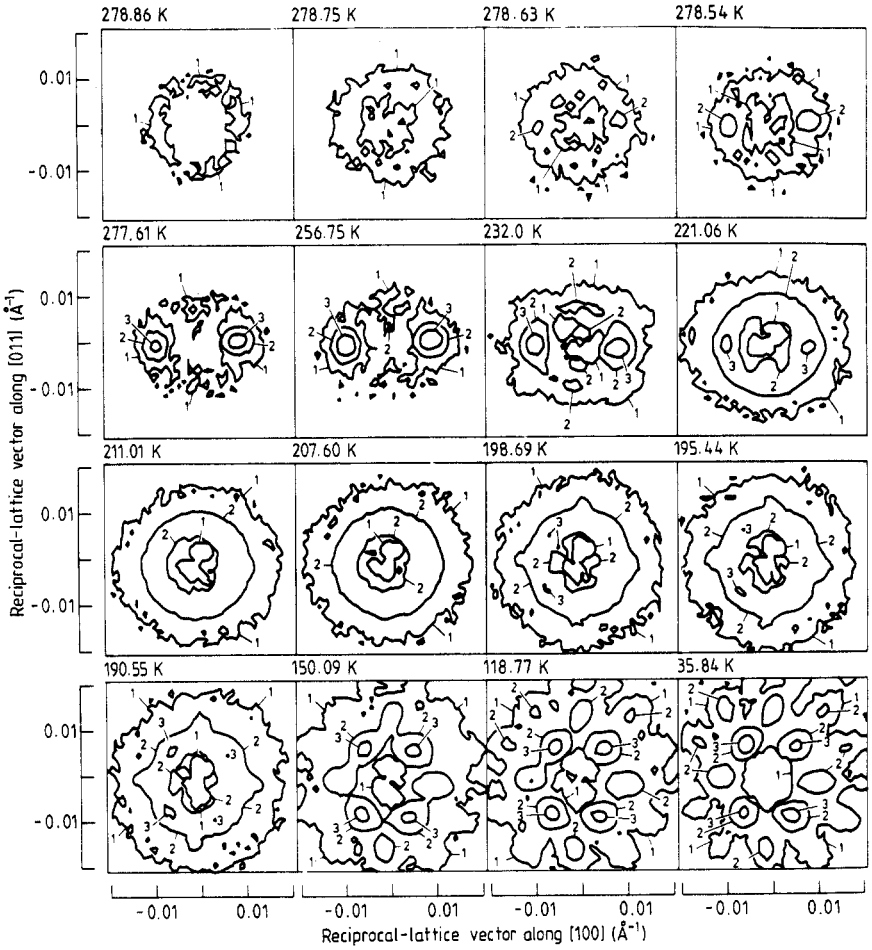

Figure 3. Equal intensity contours (logarithmic scale) observed in the $(0\bar{1}1)$ plane of cubic FeGe at various temperatures below $T_N = 278.7$ K after background subtraction and normalisation (see text). There are factors of 10 between the contour lines marked 1, 2 and 3.

the spiral at all temperatures, and the spiral may be either left- or right-handed (Bak and Jensen 1980). The crystal contains six and eight different magnetic domains at high and low temperatures, respectively. We interpret the transition starting at ~232 K (for temperature decreasing) as a turn of the spiral propagation vector from propagating along one set of symmetry directions to propagating along another set, keeping the magnetic moment perpendicular to the spiral propagation vector during the process. The appearance of the higher-order satellites may be caused either by a squaring up (or bunching) of the spiral or as multiple Bragg scattering. By comparing figure 3 and figures 2(*a*) and (*b*), it is evident that at high temperatures only first-order satellites are observed while at least first-, second- and third-order satellites are observed at the lowest temperatures.

Figure 4 shows the temperature dependence of the total intensity recorded by the area-sensitive detector for decreasing (◇) and increasing (○) temperature. Although the data show very little hysteresis at T_N (see the inset of figure 4), we conclude that the

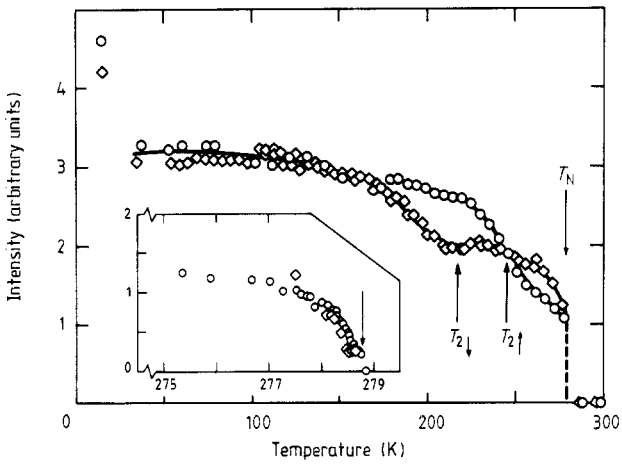

Figure 4. Temperature dependence of the total intensity recorded by the area-sensitive detector after background subtraction and normalisation to the water spectrum (see text). The inset shows the region near $T_N = 278.7$ K (shown by the arrow) on an expanded scale. There is a slight hysteresis at T_N and a much larger hysteresis at T_2 ($T_{2\downarrow} = 211$ K for temperature decreasing (◇), $T_{2\uparrow} = 245$ K for temperature increasing (○)).

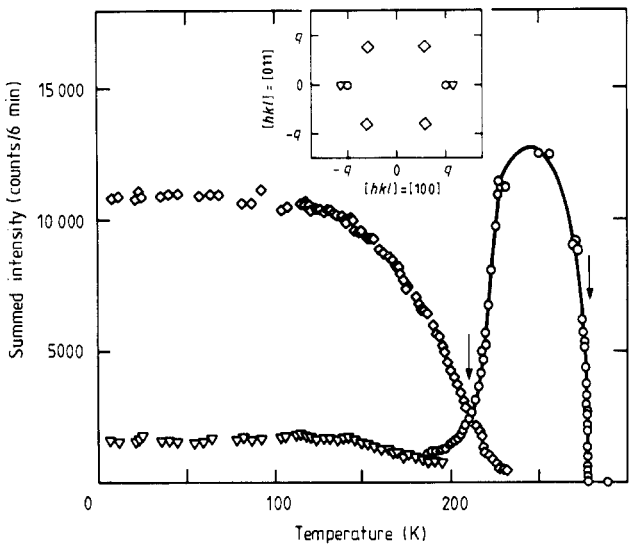

Figure 5. Temperature dependence of the integrated intensity of specific satellites (see inset) around (0, 0, 0) in cubic FeGe (temperature decreasing). The circles show the intensity in the first-order satellite at $-\boldsymbol{Q}_1 = -Q_0(1, 0, 0)$ ($Q_0 \approx 0.0090$; see figure 4), the squares the sum of the intensities in the first-order satellites at $-\boldsymbol{Q}_1 = -Q_0/\sqrt{3}(1, 1, 1)$ and $-\boldsymbol{Q}_2 = -Q_0/\sqrt{3}(1, \bar{1}, \bar{1})$, and the triangles the intensity of the second-order satellite at $-\boldsymbol{Q} = -(\boldsymbol{Q}_1 + \boldsymbol{Q}_2)$, $Q_0 \approx 0.0092$ Å^{-1} (see figure 6). The meaning of $\boldsymbol{Q}_i$ may be easier to understand by comparison with figures 2(*a*) and (*b*).

transition is first order. This conclusion is supported by the fact that the intensity in a particular satellite increases with the time spent at the same nominal temperature. The second transition is sluggish and takes place in a temperature interval of about ±20 K around T_2. The second transition shows pronounced hysteresis (see figure 4). For

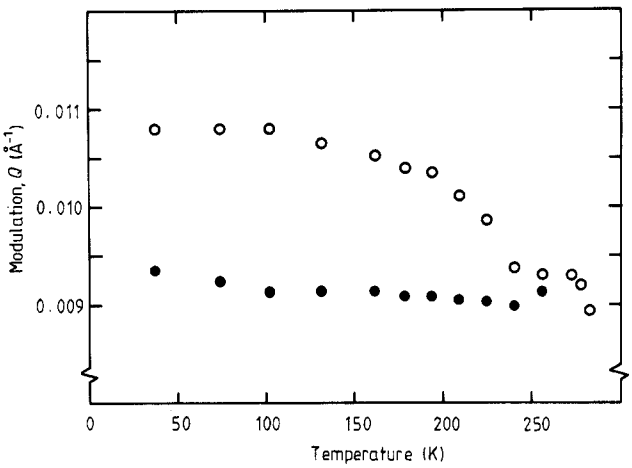

Figure 6. Temperature dependence of the modulation vector in cubic FeGe (temperature decreasing, zero applied magnetic field). Between $T_N = 278.7$ K and T_2, Q is parallel to equivalent ⟨100⟩ directions (○). Below T_2, Q is parallel to equivalent ⟨111⟩ directions (●), and second-order satellites are observed along for instance ⟨100⟩ directions (○).

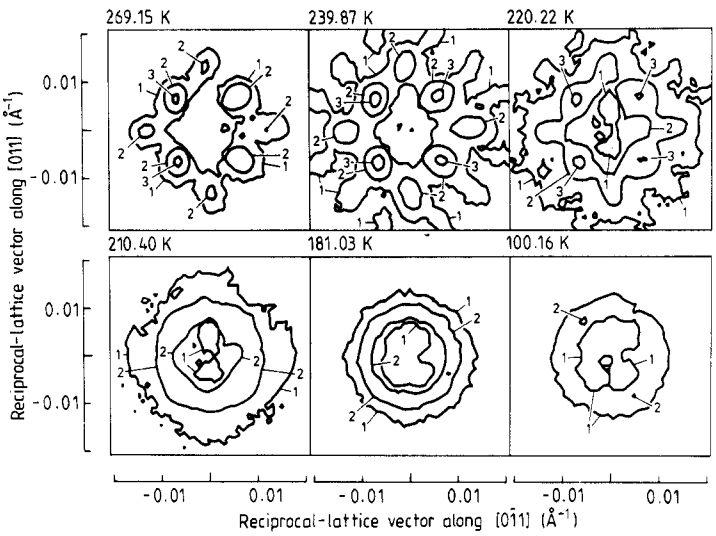

Figure 7. Equal intensity contours (logarithmic scale) observed in the (100) plane of cubic FeGe at various temperatures below $T_N = 287.7$ K after background subtraction and normalisation (see text). There are factors of 10 between the contour lines marked 1, 2 and 3.

temperature decreasing we estimate $T_{2\downarrow} = 211$ K and for temperature increasing $T_{2\uparrow} = 245$ K. Figure 5 shows the temperature dependence of the integrated intensity in some of the satellites observed around (0, 0, 0) in cubic FeGe. The intensities have been evaluated from data similar to those shown in figure 3 by summing the number of counts

(after background subtraction and normalisation) in each channel in a square lattice surrounding the given satellite. At high temperatures, the circles show the temperature dependence of the $-\boldsymbol{Q}_1 = -Q_0(1, 0, 0)$ satellite intensity. At low temperatures, the squares show the sum of the intensity of the first-order satellites at $-\boldsymbol{Q}_1 = -(Q_0/\sqrt{3})$ $(1, 1, 1)$ and $-\boldsymbol{Q}_2 = -(Q_0/\sqrt{3})(1, \bar{1}, \bar{1})$ against temperature and the triangles the temperature dependence of the second-order satellite at $-\boldsymbol{Q}' = -(\boldsymbol{Q}_1 + \boldsymbol{Q}_2)$. The temperature dependence of the sum of the intensities in the equivalent second-order satellites at $\pm\boldsymbol{Q}'' = \pm(\boldsymbol{Q}_1 - \boldsymbol{Q}_2)$ is almost coinciding with the triangles.

The temperature dependence of the length (Q) of the spiral wavevector $\boldsymbol{Q}$ was determined from radial plots along [100], [011], [111] and [$\bar{1}$11]. It shows almost no temperature dependence. The results are summarised in figure 6 which shows the components of $\boldsymbol{Q}$ along [100] and [111]. Again it is evident that at high temperature $\boldsymbol{Q}$ is along ⟨100⟩ and at low temperature $\boldsymbol{Q}$ is along ⟨111⟩. At 50 K the ratio between the $\boldsymbol{Q}$ components along [100] (○) and along [111] (●) is $2/\sqrt{3} = 1.1547$, which agrees with the assumption that, at low temperatures, the satellites observed in the ⟨100⟩ directions are higher-order satellites of first-order satellites from spirals propagating along the ⟨111⟩ directions. The same is true for instance for the satellites observed in the ⟨011⟩ directions.

The origins of the higher-order satellites were investigated in some detail. At 25 K, two-dimensional data were collected at different wavelengths (9, 11.8, 13.8, 15.8, 17.6, 19.7, 22.5 and 26 Å). At all wavelengths we observed diffraction patterns similar to that shown for 35.84 K in figure 3. Although the different satellites were not well resolved at the shortest wavelengths, it was possible to estimate the wavelength dependence of the intensity in the $\pm\boldsymbol{q}_1$ ($\pm\boldsymbol{q}_2$), $\pm(\boldsymbol{q}_1 + \boldsymbol{q}_2)$ and $\pm(\boldsymbol{q}_1 - \boldsymbol{q}_2)$ from 9 to 26 Å. The wavelength dependence of the intensities were smooth for the three types of satellite, which is inconsistent with the assumption that the higher-order satellites arise from multiple Bragg scattering. However, the two-dimensional diffraction patterns were also collected for other orientations of the crystal. An example of such data is shown in figure 7, where the sample has been rotated 90° around the vertical [011] axis as compared with figure 3. In this case, the experimental set-up corresponds to the situation illustrated in figures 2(c) and 2(d). It is striking to note that, in addition to the first-order satellites at $\boldsymbol{q} = \pm\boldsymbol{q}_2$ and $\boldsymbol{q} = \pm\boldsymbol{q}_3$, the diffraction pattern at 269.15 K shows second-order satellites corresponding to $\boldsymbol{q} = \pm(\boldsymbol{q}_2 - \boldsymbol{q}_3)$ and $\boldsymbol{q} = \pm(\boldsymbol{q}_2 + \boldsymbol{q}_3)$. This contrasts with the data taken at the former orientation at 256.75 K (figure 3) where the diffraction pattern shows only first-order satellites at $\boldsymbol{q} = \pm\boldsymbol{q}_1$. Rotation around the [011] axis corresponds to rotation around the reciprocal lattice vector $\boldsymbol{q}_2 + \boldsymbol{q}_3$ which is one experimental test for multiple Bragg scattering effects. Therefore the difference between the high-temperature data in figures 3 and 7 strongly supports the assumption that the higher-order satellites observed in cubic FeGe are caused by multiple Bragg scattering and not by modifications in the spiral magnetic structure.

A similar explanation was given for the higher-order satellites observed in MnSi (Ishikawa *et al* 1986). However, because our data are not totally consistent with the assumption of multiple Bragg scattering and because this is one of the first structural studies using small-angle neutron scattering, an attempt will be made to elucidate the problem by means of Monte Carlo computer simulation techniques. It should also be noted that the ring of scattering (of diameter q) observed at 100.16 K (figure 7) is inconsistent with the pattern expected in this orientation at low temperatures. For the data to be consistent with the low-temperature data in figure 3, only distinct second-order satellites (see figure 2(d)) or no scattering at all should have been observed. At present, we lack a satisfactory explanation for this experimental observation.

4. Experimental results in non-zero field

The effect of an applied magnetic field on the spiral structure was investigated both in the high-temperature and in the low-temperature phases for fields along the three symmetry directions. Generally it was found that even small magnetic fields (~1 mT) introduce changes in the spiral magnetic structure. Magnetic fields of 20–40 mT (depending on temperature and field direction) cause the spiral axis to turn to the direction of the applied field. During this process the total intensity remains nearly unchanged, which means that the spins remain perpendicular to the propagation direction of the spiral. As the field is further increased, the amplitude of the spiral decreases and a ferromagnetic component develops until, at fields above ~200–300 mT, the spiral structure disappears and cubic FeGe becomes magnetically saturated. When the field is reduced to zero the original spiral structure reappears. However, the diffraction pattern shows traces of the spiral structure propagating along the direction of the field indicating that the crystal is not in its 'virgin' state. As examples, typical sets of data for fields along [011] are shown in figure 8. The two right-hand columns of figure 8 show the effects of field on the diffraction patterns from the $(0\bar{1}1)$ plane (figures 2(*a*) and 8(*b*)) and the (100) plane (figures 2(*c*) and 8(*c*)) at 250 K, and the left-hand column (figure 8(*a*)) shows similar results for the $(\bar{2}\bar{1}1)$ plane (defined by the [011] and the $[\bar{1}1\bar{1}]$ reciprocal lattice vectors) at 140 K. The 0 mT data show the diffraction patterns for the 'virgin' crystal, i.e. cooled from 10 K above T_N in zero field to 250 K and 140 K, respectively.

Let us now concentrate on the data at 250 K. In zero field, we observe first-order satellites at $\boldsymbol{q} = \pm\boldsymbol{q}_i$ ($i = 1, 2, 3$) and higher-order satellites which are combinations of $\boldsymbol{q}_2$ and $\boldsymbol{q}_3$ (see figures 2(*a*) and 2(*c*)). At about 0.9 mT, second-order satellites develop at $\boldsymbol{q} = \pm 2\boldsymbol{q}_1$ (see figure 8(*b*)). There are two possible explanations for the satellites at $2\boldsymbol{q}_1$. The first is a deformation of the spiral (squaring up). The second is a growth of the domain corresponding to a spiral propagating perpendicular to the field ($\boldsymbol{q} = \boldsymbol{q}_1$, see figure 2(*a*)) at the expense of the two other domains ($\boldsymbol{q} = \boldsymbol{q}_2$ or $\boldsymbol{q} = \boldsymbol{q}_3$, see figure 2(*c*)), in which case the origin of the $\boldsymbol{q} = 2\boldsymbol{q}_1$ satellites would be multiple scattering. However, such a domain growth would mean that the intensity of the $\boldsymbol{q}_2$ and $\boldsymbol{q}_3$ satellites decreases while the intensity of the $\boldsymbol{q}_1$ and $2\boldsymbol{q}_1$ satellites increases; this is not observed (see figure 8(*c*)). Therefore, we conclude that at ~9 mT there is a true change of the magnetic structure. As the field is further increased the distinct satellites disappear at first, then the intensity deforms to concentrate predominantly along the [011] field direction until at ~25–30 mT distinct satellites appear at the [011] axis, indicating that the crystal has become one magnetic domain with the spiral propagating along the field direction. Already at 40 mT there is evidence of a ferromagnetic component as well (cone structure). This may be seen by comparing the scattering near the origo at 0 mT and 44.1 mT (figures 8(*a*) and 8(*c*)). At 0 mT there is no intensity near the origo while there is a finite intensity at 44.1 mT, although the central part of this intensity is absorbed by the beam stop.

Figure 9 shows as an example the field dependence of the intensity in the three main satellites observed in the $(0\bar{1}1)$ plane (figure 8(*b*)) for field along [011] at 250 K. As mentioned above, the $\langle q, 0, 0\rangle$-type satellites are the only satellites present at zero field, but already at 2 mT second-order satellites ($\langle 2q, 0, 0\rangle$-type) appear. Both types of satellite decrease in intensity above 10 mT, where the satellites with wavevector $\boldsymbol{q} \parallel \boldsymbol{B}$ start to grow to reach saturation at ~20 mT. As the field is further increased there is a steady decrease of these satellites and an associated increase of ferromagnetic intensity at the origo. As mentioned previously, this intensity cannot be monitored because its central part is hidden by the beam stop.

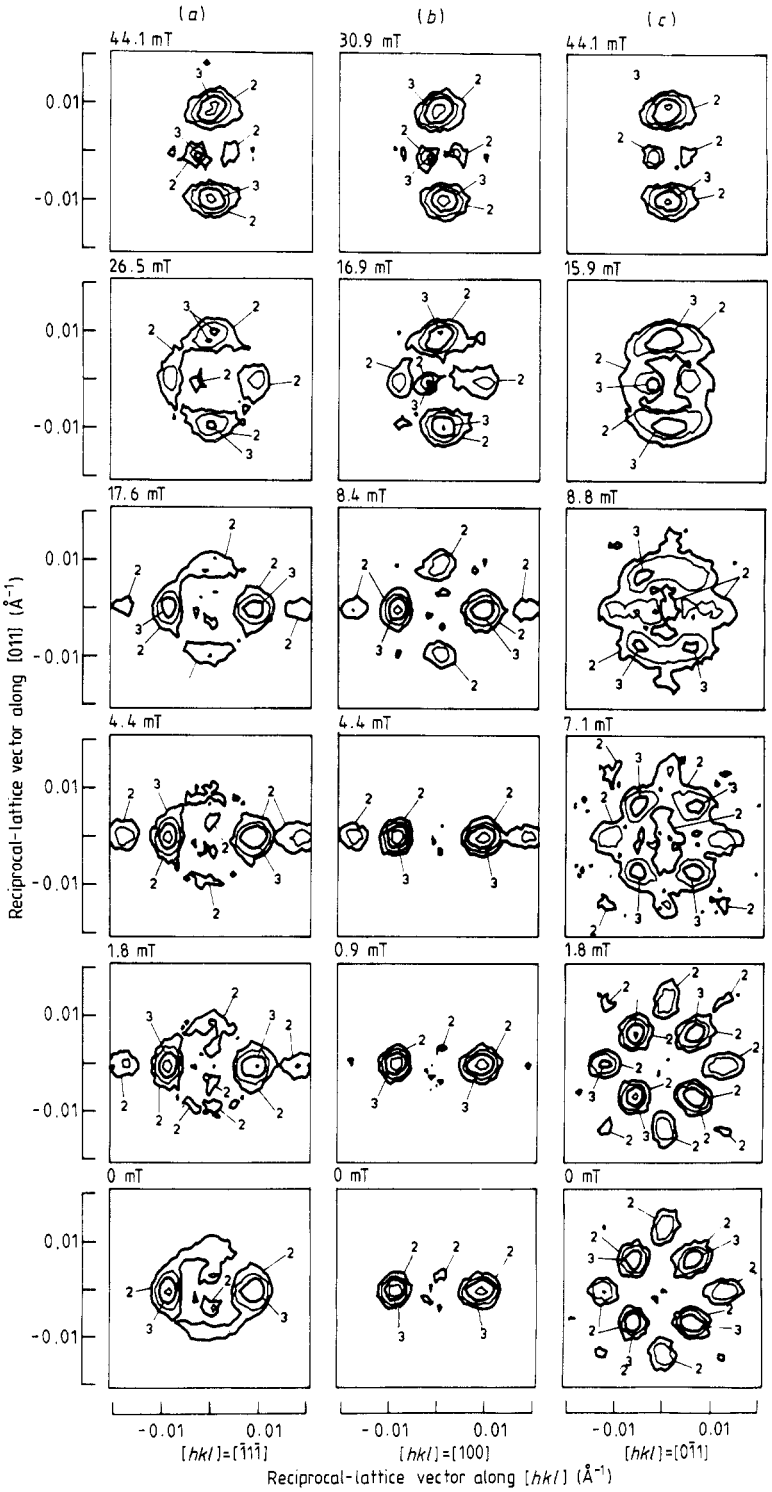

Figure 8. Equal intensity contours (logarithmic scale) observed in cubic FeGe (*a*) at 140 K, (*b*) at 250 K in the $(0\bar{1}1)$ plane and (*c*) at 250 K in the (100) plane for various magnetic fields applied along the [011] vertical direction. The background has been subtracted and the data normalised (see text). There are factors of 10 between the contour lines marked 1 and 2.

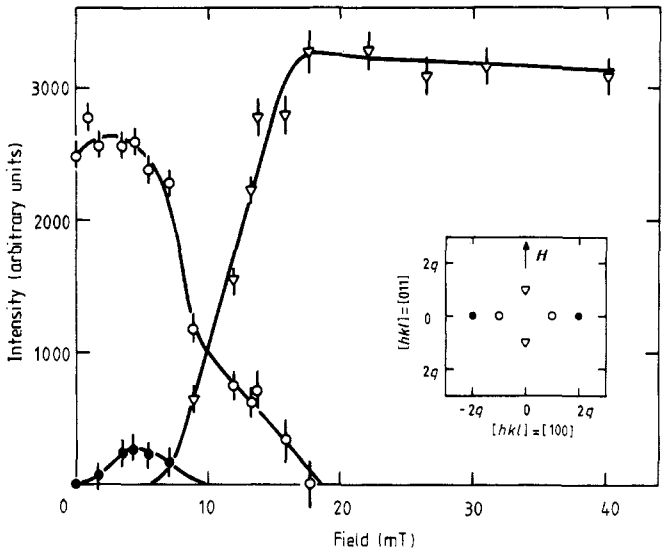

Figure 9. Field dependence ($H \| [011]$) at 250 K of the integrated intensity in specific satellites (see inset) around (0, 0, 0) in cubic FeGe. Shown are the intensities of the first-order satellites at $\pm \boldsymbol{Q}_1 = \pm Q_0\,(1, 0, 0)$ ($Q_0 = 0.0090$ Å^{-1}; see figure 11(a) (○), the intensities of the second-order satellites at $\pm 2\boldsymbol{Q}_1$ (●), and the intensities appearing in the field direction above ~8 mT at $\pm(Q_0/\sqrt{2})\,(0, 1, 1)$ (▽).

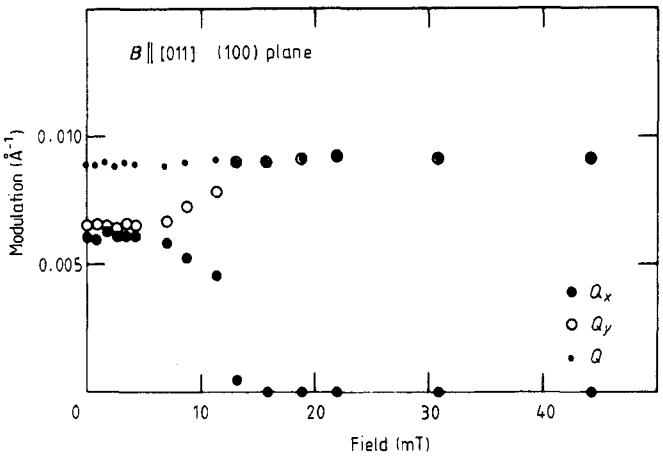

Figure 10. Field dependence of the modulation wavevector in cubic FeGe at 250 K for a field applied in the vertical [011] direction. The wavevector $\boldsymbol{Q} = (Q_x, Q_y, 0)$ is determined from Q_x along $[0\bar{1}1]$ and Q_y along [011]. The [100] axis is in the direction of the incident beam (see figures 2(c) and 2(d)). At low fields $\boldsymbol{Q} \| \langle 100 \rangle$, above 13 mT $\boldsymbol{Q} \| [011]$.

The turn of the spiral wavevector $\boldsymbol{Q}$ in a magnetic field is illustrated in more detail in figures 10 and 11. The data in figures 10 and 11(a) may be directly related to the contour diagrams shown in figures 8(b) and 8(c). Figure 10 shows the field dependence in the (100) plane of $\boldsymbol{Q}_3 = (Q_x, Q_y, 0)$ at 250 K (figures 2(c) and 8(c)), where Q_x is the component along the $[0\bar{1}1]$ and Q_y the component along the [011] axis. Up to ~8 mT the

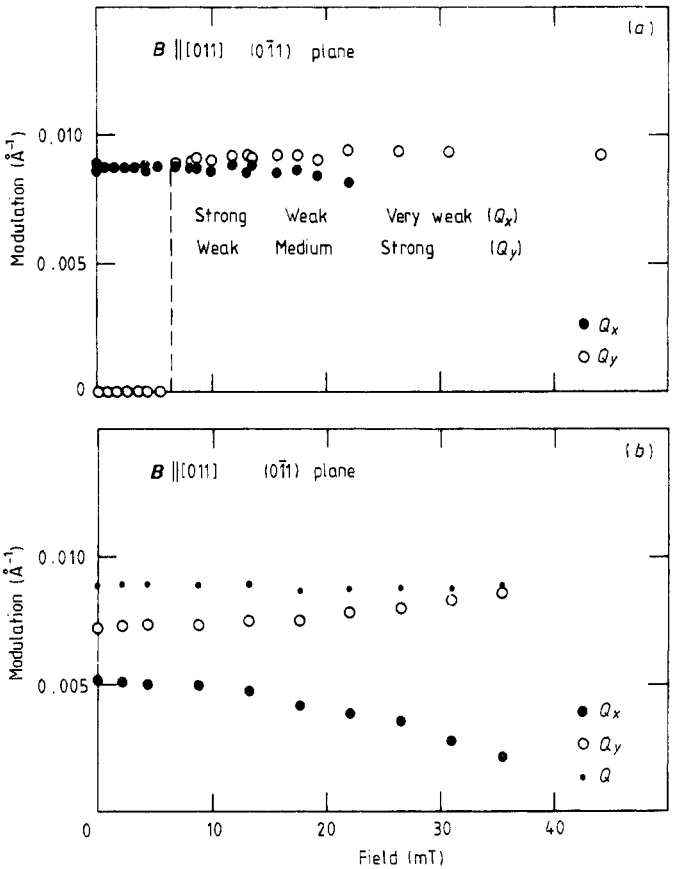

Figure 11. Field dependence of the modulation wavevector in cubic FeGe for a field applied in the vertical [011] direction at (*a*) 250 K and (*b*) 140 K. The wavevector $Q = (Q_x, Q_y, 0)$ is determined from Q_x along [100] and Q_y along [011]. The [0$\bar{1}$1] is in the direction of the incident beam (see figures 2(*a*) and 2(*b*)). At both temperatures Q turns toward the field direction, the low-temperature phase ($\boldsymbol{Q}\|\langle 111\rangle$) being magnetically more hard than the high-temperature phase ($\boldsymbol{Q}\|\langle 100\rangle$). The text in figure 11(*a*) refers to the intensity of the satellites at $(Q_x, 0, 0)$ and $(0, Q_y, 0)$, respectively.

spiral wavevector stays along $\boldsymbol{Q}_3 = Q_0\,(0, 0, 1)$ ($Q_0 = 0.0090$ Å^{-1}); thereafter $\boldsymbol{Q}$ slowly turns towards the [011] field direction which is reached at ~18 mT. The field dependence for $\boldsymbol{Q}_2$ is similar (see figures 2(*c*) and 8(*c*)).

Figure 11 shows the same development in the (0$\bar{1}$1) plane. In this case Q_x measures the component along the [100] and Q_y the component along the [011] direction. At 250 K (figure 11(*a*)), we only observe satellites in the [100] direction ($\pm\boldsymbol{Q}_1 = (Q_x, 0, 0)$ and $\pm 2\boldsymbol{Q}_1$) up to ~7 mT. Above 7 mT, these satellites slowly decrease in intensity with very little change in their position. Above ~25–30 mT these satellites have disappeared. While the satellites at $\boldsymbol{Q}_1$ decrease in intensity, satellites develop at $\boldsymbol{Q} = \pm(0, Q_y, 0)$ where $Q_y \simeq 0.0090$ Å^{-1}, to reach their maximum intensity at ~30 mT. At 140 K the wavevectors are parallel to equivalent ⟨111⟩ directions. As the field is increased they slowly turn towards the field direction, which is reached at ~40 mT for field along [011]. This is illustrated in figure 11(*b*) which shows the behaviour of the satellites with

wavevector $\boldsymbol{Q} = Q\,[\bar{1}, 1, \bar{1}]$ ($Q_x/Q_y = \sqrt{2}$). Although the data in figures 8(*a*) and 11(*b*) show the field dependence of the ⟨111⟩-type of satellites (figure 8(*a*) shows $\boldsymbol{Q}_3(H)$ and figure 11(*b*) $\boldsymbol{Q}_1(H)$), these figures may not be directly related. However, they lead to the same conclusions about the field dependence of the spiral structure at 140 K.

5. Summary and discussion

The present small-angle neutron scattering studies of the cubic polymorph of FeGe have shown that, in zero field, the magnetic structures are long-range spirals which propagate along equivalent ⟨100⟩ directions between $T_N = 278.7$ K and T_2, where $T_{2\downarrow} = 211$ K for decreasing temperature and $T_{2\uparrow} = 245$ K for increasing temperature. Below T_2, the magnetic structures are long-range spirals which propagate along equivalent ⟨111⟩ directions. The spin structure can be expressed as

$$\boldsymbol{S}(\boldsymbol{r}) = \boldsymbol{M}_Q \cos(\boldsymbol{Q}\cdot\boldsymbol{R}) - \boldsymbol{N}_Q \sin(\boldsymbol{Q}\cdot\boldsymbol{R}) \tag{1}$$

where $\boldsymbol{Q} = Q_0\langle 100\rangle$ ($Q_0 = 0.0090$ Å^{-1}) in the high-temperature phase and $\boldsymbol{Q} = (Q_0/\sqrt{3})\langle 111\rangle$ ($Q_0 = 0.0092$ Å^{-1}) in the low-temperature phase. Presumably, this difference corresponds to a corresponding change in lattice parameter. In equation (1) $\boldsymbol{M}_Q \perp \boldsymbol{N}_Q$, $|\boldsymbol{M}_Q| = |\boldsymbol{N}_Q|$ and $\boldsymbol{Q} \| \boldsymbol{M}_Q \times \boldsymbol{N}_Q$. Because the measurements were made using small-angle neutron scattering, no nuclear reflections could be observed. Therefore, no attempt was made to bring the intensities on an absolute scale, and hence the amplitude (ordered moment) of the spiral could not be estimated. The transition at T_N was found to be first order, whereas the transition at T_2 is rather sluggish and takes place over a temperature range of ±20 K around T_2. The transition at T_2 showed large thermal hysteresis. At T_N, very little thermal hysteresis was observed, but a notable ring of diffuse scattering was observed at a distance Q_0 from the origo just above T_N. Magnetic fields of a few mT in any direction and at any temperature below T_N were found to cause considerable changes in the magnetic structure. Magnetic fields of ~20–40 mT caused the spiral propagation vector to turn into the field direction. At fields above ~50 mT a cone structure develops. The propagation vector remains along the field direction until the structure becomes ferromagnetic above 200–400 mT. The length of the spiral wavevector $\boldsymbol{Q}$ is nearly independent of temperature and field.

The results for cubic FeGe in applied magnetic fields are similar to those reported by Ishikawa and Arai (1984) for the isostructural compound MnSi. They are also consistent with the conclusion of Haraldson *et al* (1978) that FeGe (and MnSi) are compounds in which every direction is magnetically hard. However, the neutron diffraction studies show that MnSi and cubic FeGe have significantly different temperature dependencies of the magnetic ordering. First of all their ordering temperatures differ by an order of magnitude; MnSi orders at 29.5 K and cubic FeGe at 278.7 K. Secondly, MnSi orders in a spiral structure propagating along equivalent ⟨111⟩ at all temperatures below T_N (Ishikawa and Arai 1984 and references therein). In contrast, the magnetic ordering in cubic FeGe exhibits two spirals, one above T_2 propagating along equivalent ⟨100⟩ directions and one below T_2 propagating along equivalent ⟨111⟩ directions ($T_{2\downarrow} = 211$ K, $T_{2\uparrow} = 245$ K). In both compounds a precursor of the magnetic ordering is observed above T_N as a ring of diffuse scattering around the origin. The radius of this ring is equal to the ordering wavevector $\boldsymbol{q}$, which is nearly independent of temperature ($\boldsymbol{Q} = 0.0362$ Å^{-1} for MnSi and $\boldsymbol{Q} = 0.0092$ Å^{-1} for cubic FeGe). Thus the systems are clearly frustrated just before ordering sets in, and it would seem plausible that MnSi

Table 1. Summary of some of the magnetic properties of cubic (B20) $T_xCo_{1-x}Si$ (T = Mn, Fe) and FeGe.

Compound	No. of 3d electrons per atom	Magnetism	T_N (K)	T_2 (K)	Q (Å^{-1})	Q direction	Reference
MnSi	25	Para/helix	29.5		0.0362	⟨111⟩	[a]
FeSi	26	Para					[b]
CoSi	27	Dia					[c]
Mn0.98Co0.02Si	25.04	Para/helix			0.0439		[d]
Mn0.9Co0.04Si	25.08	Para/helix			0.0593		[d]
Fe0.9Co0.1Si	26.1	Para/helix	21.3		0.0146		[d,e]
Fe0.8Co0.2Si	26.2	Para/helix	34.7		0.0213		[e]
Fe0.65Co0.35Si	26.35	Para/helix	58.8		0.0133		[d,e]
Fe0.5Co0.5Si	26.5	Para/helix	43.5		0.0077		[d,e]
Fe0.4Co0.6Si	26.6	Para/helix			0.0036		[d,e]
Fe0.3Co0.7Si	26.7	Para/helix	8.8		0.0027		[d,e]
FeGe	26	Para/helix	278.7	211 ↓, 245 ↑	0.0092	⟨100⟩, ⟨111⟩	Present work

[a] Ishikawa *et al* (1976), Hansen (1977).
[b] Wertheim *et al* (1965).
[c] Amamou *et al* (1972).
[d] Beille *et al* (1983).
[e] Beille *et al* (1981).

could order with ⟨100⟩-type spirals in a very narrow temperature range below T_N. We looked for this type of order in MnSi without success. Thus we conclude that only one type of spiral exists in MnSi while two types of spiral exist in cubic FeGe.

The spiral magnetic structures observed in MnSi and cubic FeGe are very long range with repeat distances of ~175 and ~700 Å, respectively. This means that they are nearly ferromagnetic and relatively small magnetic fields are needed to reach magnetic saturation. So far only MnSi and cubic FeGe have been studied in single crystalline form, but spirals of even longer range have been observed in powders of the isostructural alloys $Fe_xCo_{1-x}Si$. Table 1 summarises some of the magnetic properties of $T_xCo_{1-x}Si$ (T = Mn, Fe) and cubic FeGe. FeSi is paramagnetic at all temperatures, but a small amount of Co stabilises the long-range spiral. As the amount of Co is increased, the repeat distance reaches a minimum of 295 Å for 20% Co; thereafter it increases to ~2300 Å at 70% Co (Beille *et al* 1981, 1983). From a plot of T_N against the number of 3d electrons we estimate that $Fe_xCo_{1-x}Si$ is paramagnetic for $x > 0.96$ and diamagnetic for $x < 0.26$. A similar estimate cannot be made for $Mn_xCo_{1-x}Si$, but it would be extremely interesting also to study the magnetic ordering in $Mn_xCo_{1-x}Si$ ($x < 0.55$), which corresponds to alloys having the same number of 3d electrons as $Fe_xCo_{1-x}Si$. It is remarkable that the minimum in the repeat distance for $Fe_xCo_{1-x}Si$ coincides with the maximum in the Slater–Pauling curve (Bozorth 1951).

Nakanishi *et al* (1980) and Bak and Jensen (1980) made a symmetry analysis of the $P2_13$ structure of MnSi and FeGe and showed, as previously mentioned, that the long-range spiral (equation (1)) in MnSi and FeGe is a consequence of the Dzyaloshinskii instability (Dzyaloshinskii 1964). Bak and Jenson (1980) further showed that the spirals would propagate along ⟨111⟩ for $B_2 < 0$ and along ⟨100⟩ for $B_2 > 0$, where B_2 is the second-order gradient in the free energy expansion. Hence it seems that in FeGe $B_2 > 0$ at high temperatures and $B_2 < 0$ at low temperatures, whereas for MnSi $B_2 < 0$ below T_N.

Lundgren *et al* (1970) measured the anisotropy constants K_1 and K_2 in cubic FeGe at 4.2, 77, 251 and 273 K. They found that at low temperatures $K_2/K_1 \sim -2$, whereas at high temperatures $K_2/K_1 \simeq -5$ to -6. Using the expression of Lundgren *et al* (1970) for the anisotropy energy U_K in zero field and their experimental values $K_1(T)$ and $K_2(T)$ for the anisotropy constants, we find that at low temperatures the type-⟨111⟩ spiral is energetically more favourable than spirals of type ⟨110⟩ or ⟨100⟩. However, at high temperatures the anisotropy energies of all three spirals approach each other, and it is not unlikely that a detailed theory or more precise measurements of the anisotropy constants would result in a crossover from the type-⟨111⟩ spiral to the type-⟨100⟩ spiral as found experimentally by our small-angle neutron scattering experiments. Therefore, it would be of interest to measure the anisotropy constants of cubic FeGe in a wide temperature range close to T_2 (i.e. 200–260 K).

Acknowledgments

One of us (BL) is grateful to Per Bak and Mogens Høgh Jensen for inspiration and many stimulating discussions. JB gratefully acknowledges economic support from the Nordic Council (Nordiska Forskar Kurser) and from Ewers and Co's foundation for Swedish scientists' studies in Denmark.

References

Amamou A, Bach P, Gautier F and Robert C 1972 *J. Phys. Chem. Solids* **33** 1697
Bak P and Jensen M H 1980 *J. Phys. C: Solid State Phys.* **13** L881
Beille J, Voiron J and Roth M 1983 *Solid State Commun.* **47** 399
Beille J, Voiron J, Towfiq F, Roth M and Zhang Z Y 1981 *J. Phys. F: Met. Phys.* **11** 2153
Bernhard J, Lebech B and Beckman O 1984 *J. Phys. F: Met. Phys.* **14** 2379 and references therein
—— 1988 *J. Phys. F.: Met. Phys.* **18** 539
Bloch D, Voiron J, Jaccarino V and Wernich J H 1975 *Phys. Lett.* **51A** 259
Bozorth R M 1951 *Ferromagnetism, The Bell Telephone Laboratories Series* (New York: Van Nostrand) p 441
Date M, Okuda K and Kadowaki K 1977 *J. Phys. Soc. Japan* **42** 1555
Dzyaloshinskii I E 1964 *J. Exp. Theor. Phys.* **46** 1420 (1964 *Sov. Phys.–JETP* **19** 960)
Ericsson T, Karner W, Häggström L and Chandra K 1981 *Phys. Scr.* **23** 1118
Felcher G P, Jorgensen J D and Wäppling R 1983 *J. Phys. F: Met. Phys.* **8** 2195
Fruchart D, Malaman B, Le Caër G and Roques B 1983 *Phys. Status Solidi* a **78** 555
Hansen P Å 1977 *Risø Report No 360*
Haraldson S, Pettersson L and Bhagat S M 1978 *J. Magnetic Resonance* **32** 115
Ishikawa Y and Arai M 1984 *J. Phys. Soc. Japan* **53** 2726
Ishikawa Y, Furusaka M, Niimura N, Arai M and Hasegawa K 1986 *J. Appl. Cryst.* **19** 229
Ishikawa Y, Komatsubara T and Bloch D 1977 *Physica* B **86–88** 401
Ishikawa Y, Tajima K, Bloch D and Roth M 1976 *Solid State Commun.* **19** 525
Kjems J K, Bauer R, Breiting B and Thuesen A 1985b *Proc. Conf. on Neutron Scattering in the Nineties, Jülich, 1985* (Vienna: IAEA) p 489
Kjems J K, Bauer R, Christensen P, Freltoft T, Jensen L G and Linderholm J 1985a *Proc. Conf. on Neutron Scattering in the Nineties, Jülich, 1985* (Vienna: IAEA) p 495
Kusaka S, Yamamoto K, Komatsubara T and Ishikawa Y 1976 *Solid State Commun.* **20** 925
Lebech B and Hansen P Å 1977 unpublished
Levinson L M, Lander G H and Steinitz M O 1978 *AIP Conf. Proc.* **10** (New York: AIP) p 1138
Lundgren L, Blom K Å and Beckman O 1968 *Phys. Lett.* **28A** 175
Lundgren L, Beckman O, Attia V, Bhattacherjee S P and Richardson M 1970 *Phys. Scr.* **1** 69
Nakanishi O, Yanase A, Hasegawa A and Kataoka M 1980 *Solid State Commun.* **35** 995
Pauling L and Soldate A M 1948 *Acta Crystallogr.* **1** 212
Plumer M L and Walker M B 1981 *J. Phys. C: Solid State Phys.* **14** 4689
Richardson M 1967 *Acta Chem. Scand.* **21** 2305
Sakakibara T, Morimoto H and Date M 1982 *J. Phys. Soc. Japan* **51** 2439
Wäppling R and Häggström L 1968 *Phys. Lett.* **28A** 173
Wilkinson C, Sinclair F and Forsyth J B 1976 *5th Int. Conf. on Solid Compounds of Transition Elements, Uppsala, Sweden, 21–25 June, 1976* (extended abstract)
Wertheim G K, Jaccarino V, Wernick J H, Seitchick J A, Williams H J and Sherwood R C 1965 *Phys. Lett.* **18** 89